

A two-step simulation methodology for modelling stagnation flame synthesised aggregate nanoparticles

Casper S. Lindberg^{1,3}, Manoel Y. Manuputty^{1,3}, Jethro Akroyd^{1,3}, Markus
Kraft^{1,2,3}

released: 10 July 2018

¹ Department of Chemical Engineering
and Biotechnology
University of Cambridge
Philippa Fawcett Drive
Cambridge, CB3 0AS
United Kingdom
E-mail: mk306@cam.ac.uk

² School of Chemical and Biomedical
Engineering
Nanyang Technological University
62 Nanyang Drive
6357459
Singapore

³ Cambridge Centre for Advanced Research
and Education in Singapore (CARES)
CREATE Tower, 1 Create Way
138602
Singapore

Preprint No. 204



Keywords: Stagnation flame, Population balance, Detailed particle model, Titanium dioxide, TTIP

Edited by

Computational Modelling Group
Department of Chemical Engineering and Biotechnology
University of Cambridge
Philippa Fawcett Drive
Cambridge CB3 0AS
United Kingdom

E-Mail: c4e@cam.ac.uk

World Wide Web: <http://como.ceb.cam.ac.uk/>

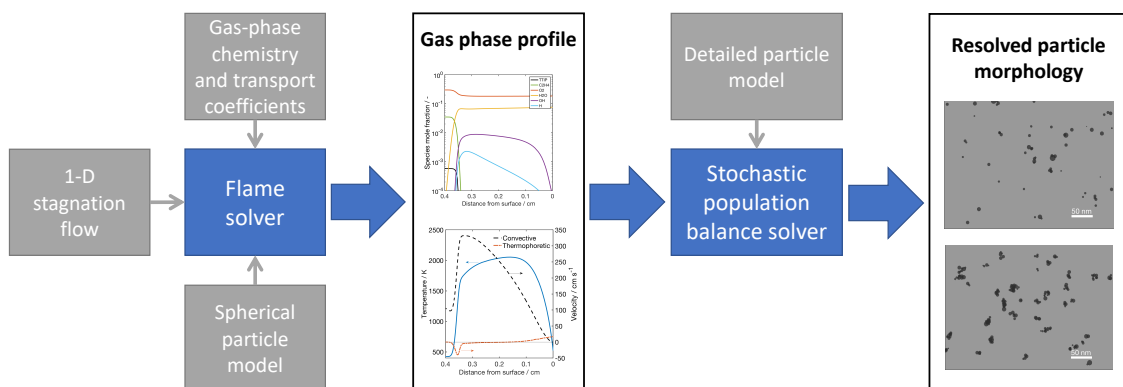


Highlights

- A two-step simulation methodology is presented for resolving the detailed morphology of stagnation flame synthesised nanoparticles.
- The methodology facilitates simulation of quantities directly comparable to experimental observations e.g. TEM images.
- A correction is introduced to the post-process to account for thermophoretic transport effects arising due to a steep temperature gradient.

Abstract

A two-step simulation methodology for modelling the stagnation flame synthesis of aggregate nanoparticles is presented. In the first step, a detailed chemical mechanism is coupled with a one-dimensional stagnation flow model and spherical particle model solved by method of moments with interpolative closure. The resulting gas-phase profile is post-processed with a detailed stochastic population balance model to simulate the evolution of the population of particles, including the evolution of each individual primary particle and their connectivity with other primaries in an aggregate. The particles evolve through surface growth, coagulation and sintering. A thermophoretic correction is introduced to the post-processing step as a simulation volume scaling term to account for thermophoretic transport effects arising due to the steep temperature gradient near the stagnation surface. The methodology is evaluated by applying it to the combustion synthesis of titanium dioxide from titanium tetraisopropoxide (TTIP) precursor. The feasibility of the methodology is demonstrated for simulating the complex aggregate morphology of stagnation flame synthesised nanoparticles and modelling quantities that are directly comparable to experimental observations.



Contents

1	Introduction	3
2	Burner configuration	4
3	Model description	5
3.1	Flow model	5
3.2	Chemical reaction model	5
3.3	Particle model	5
3.3.1	Spherical particle model	5
3.3.2	Detailed particle model	5
4	Methodology	7
4.1	Two-step simulation methodology	7
4.2	Particle population governing equations	8
4.2.1	First simulation	8
4.2.2	Second simulation	8
4.2.3	Thermophoretic correction	9
4.3	Simulated TEM images	10
5	Results and Discussion	10
5.1	Transport terms	10
5.2	Post-processing method evaluation	11
5.3	Detailed particle model application	14
6	Conclusions	15
7	Acknowledgements	16
	References	17

1 Introduction

Combustion synthesis is a key route for nanoparticle production that has received significant focus in the research community. A common strategy to understand and optimize the synthesis process is to develop comprehensive models of the combustion system guided by experimental observations. In this paper, we develop a simulation methodology for modelling aggregate nanoparticles in a stagnation flame. The simulation methodology is applied to the example of the combustion synthesis of titanium dioxide (TiO_2) nanoparticles from titanium tetraisopropoxide (TTIP) precursor. TiO_2 particles are an important industrial product and their functionality is strongly influenced by the morphology and crystalline phase of the particles.

Various deterministic methods have been applied to solve the particle dynamics after TiO_2 is formed from the gas-phase with varying levels of detail in the particle description. These include moving sectional methods [27, 28], bimodal log-normal moment methods [13], and method of moments with interpolative closure (MoMIC) [18]. However, these methods are generally limited in terms of type space (i.e. the number of internal particle dimensions) that can be tracked.

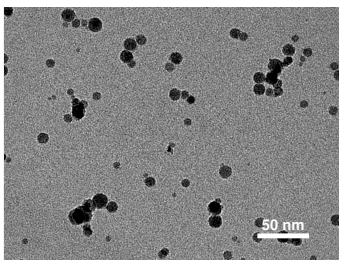


Figure 1: A typical experimental TEM image of stagnation flame synthesised TiO_2 .

Flame synthesised TiO_2 particles are often aggregate particles composed of polydisperse primary particles such as those shown in Fig. 1. A detailed description of the aggregate particle morphology is therefore necessary to simulate quantities that are directly comparable with experimental observations. Stochastic methods allow for the extension of the particle model to include a very detailed description of each particle. Detailed particle models have been developed for soot [31], silicon [20], silica [24] and TiO_2 [3, 17]. Xu et al. [30] recently used a stochastic method to model TiO_2 particle dynamics with phase transformation.

Premixed stagnation flame experiments have been used to synthesise ultra-fine TiO_2 nanoparticles from TTIP [19, 26]. The small particle size, a result of a very short particle residence time, makes these experiments suitable for studying the early stages of particle formation. In addition, the pseudo one-dimensional flow makes it easier to couple the particle model with the gas-phase chemistry and flow dynamics.

The purpose of this paper is to present a two-step simulation methodology able to resolve the complex aggregate morphology of nanoparticles synthesised in a stagnation flame. The methodology is presented in the context of TiO_2 particle synthesis, but is equally applicable to other nanoparticles formed in stagnation flames. The first step in the

method couples detailed gas-phase chemistry, flow and a spherical particle model solved by MoMIC to simulate the flame profile and particle moments. In the second step, the flame profile is post-processed with a detailed particle model capable of tracking individual primary particle coordinates, solved using a stochastic numerical method. The detailed particle description facilitates comparison with experimental observation such as TEM images. Furthermore, morphology dependent processes such as sintering and phase transformation can be studied.

A similar post-processing technique has been used successfully to simulate soot formation in premixed laminar flames with no stagnation surface [2, 7, 21, 23, 25]. Yapp et al. [31] applied this technique to model soot formation in a stagnation flame, but found that the simulations did not reproduce the experimental particle size distribution (PSD) data well. While some of the differences can be attributed to uncertainties in the models used, the results also suggest that the post-processing methodology employed is unsuitable in cases with strong temperature gradients and significant thermophoretic transport effects. In this paper we discuss how the steep temperature gradient at the stagnation surface requires a generalisation of the methodology to account for thermophoresis in the post-process. Furthermore, we introduce a correction to the post-process through a modified simulation sample volume scaling term.

2 Burner configuration

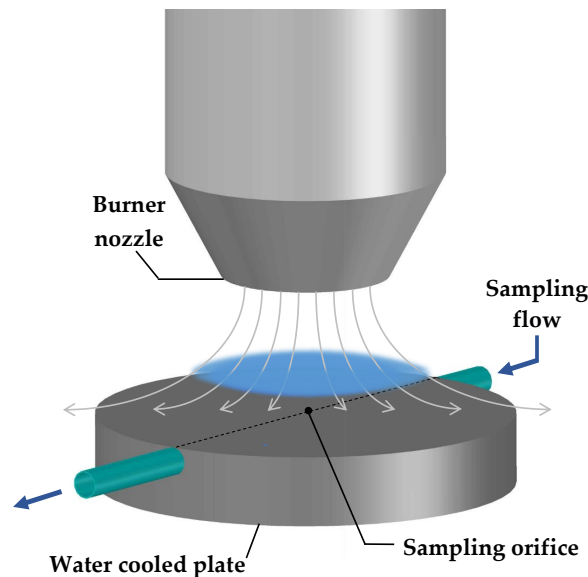


Figure 2: *Schematic of experimental set-up being modelled.*

A premixed laminar stagnation flame is modelled in this study. The set-up, shown in Fig. 2, is similar to that used in previous studies of titania and soot formation [6, 19, 26]. An aerodynamic nozzle issues a laminar jet of TTIP-doped premixed $C_2H_4/O_2/Ar$ that impinges on a water-cooled stagnation plate. A thin flame is formed and stabilised by

stretch above the surface. Particles are sampled through an orifice at the centre of the plate.

3 Model description

3.1 Flow model

The flow is assumed to be an axisymmetric stagnation flow and is modelled using a pseudo one-dimensional approximation. This is described in detail by Manuputty et al. [18].

3.2 Chemical reaction model

The chemical model consists of a TTIP decomposition mechanism combined with hydrocarbon combustion chemistry described by the USC-Mech II model [29]. The TTIP decomposition model contains 25 Ti species and 65 reactions, and describes two of the main decomposition pathways identified by Buerger et al. [5]. The decomposition product for both pathways is titanium hydroxide ($\text{Ti}(\text{OH})_4$), which is treated as the collision species for the particle inception and condensation reactions in the particle model.

3.3 Particle model

The mathematical description of a particle is called the type-space. In this work we use a spherical and a detailed type-space. The dynamics of the particle population are described by the Smoluchowski coagulation equation with additional terms for inception, condensation and sintering (detailed model only) [15]. A separate work with a comprehensive description of the detailed model type-space and particle processes is in preparation, so only a brief summary is given here.

3.3.1 Spherical particle model

The spherical particle model characterises a particle using its number of constituent TiO_2 monomers, i . The particle mass is $i \cdot m_{\text{TiO}_2}$, where m_{TiO_2} is the mass of a single monomer of TiO_2 ; and, assuming spherical geometry the particle diameter can be calculated. The collision limited inception and condensation processes are the same in both spherical and detailed particle models, and are outlined below. The particle models differ primarily in their treatment of a coagulation event: the spherical model effectively assumes instantaneous coalescence following the collision.

3.3.2 Detailed particle model

The type-space of the detailed particle model is illustrated in Fig. 3. An aggregate particle is composed of polydisperse primary particles modelled as overlapping spheres based on

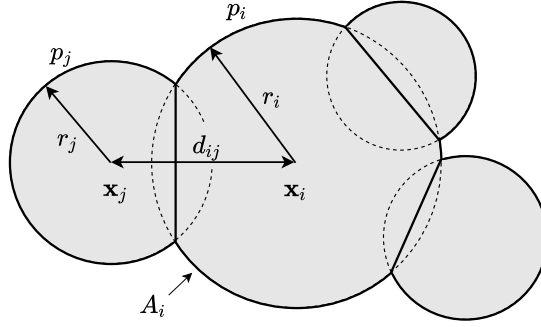


Figure 3: An illustration of the detailed particle model type space showing an aggregate particle composed of primary particles (solid outlines) modelled as overlapping spheres (indicated by dashed lines).

the approach of Eggersdorfer et al. [9, 10]. Each primary particle, p_i , is characterised by its radius, r_i , and by the position of the primary centre relative to the centre of mass of the aggregate, \mathbf{x}_i . The degree of overlap between two neighbouring primaries, p_i and p_j , is resolved by their centre to centre separation, $d_{ij} = |\mathbf{x}_i - \mathbf{x}_j|$.

Inception is modelled as a bimolecular collision of two $\text{Ti}(\text{OH})_4$ molecules forming a particle consisting of a single primary. The rate is given by the free molecular collision kernel [24] with the $\text{Ti}(\text{OH})_4$ collision diameter calculated from the geometrical parameters calculated by Buerger et al. [4].

An aggregate is formed when two particles (single primary or aggregate) stick together as a result of a collision. The rate of coagulation is calculated using a transition kernel [23, 24]. The orientations of the colliding particles and point of contact following the collision are determined by ballistic cluster-cluster aggregation with a random impact parameter [14].

A particle may grow via condensation due to a collision, assumed to take place in the free molecular regime, between a molecule of $\text{Ti}(\text{OH})_4$ and the particle with the release of two H_2O molecules. The condensing mass is added to a constituent primary particle, p_i , selected with probability proportional to its free surface area, A_i , normalised by the free surface area of the aggregate.

Neighbouring primary particles undergo rounding via a sintering process in which the primary centres approach each other increasing their overlap. Mass is conserved by increasing the primary radii. The sintering model follows the approach of Eggersdorfer et al. [10] with the rate evaluated using the grain boundary diffusion model. Once sufficiently sintered, two primaries are assumed to coalesce into a single primary.

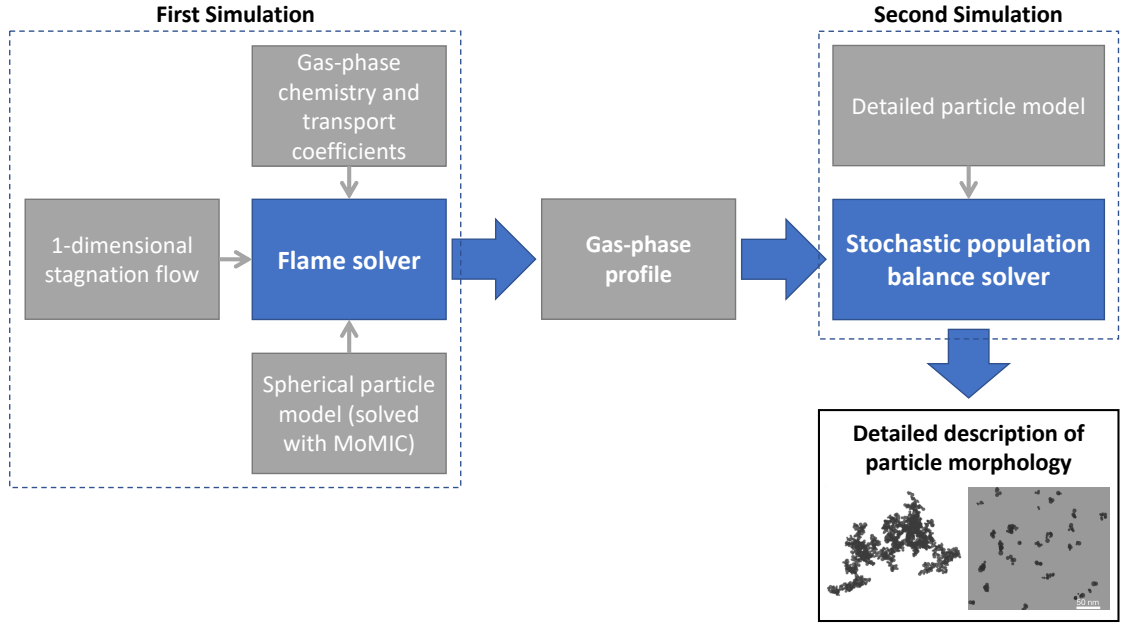


Figure 4: *Two-step simulation methodology.*

4 Methodology

4.1 Two-step simulation methodology

Figure 4 illustrates the two-step simulation methodology employed. In the first step, the flame is simulated with a one-dimensional stagnation flow approximation, coupled with gas-phase chemistry (Section 3.2) and a spherical particle model (Section 3.3.1) solved with method of moments with interpolative closure (MoMIC). This is solved as a boundary-value problem using the *kinetics*[®] software package [8] with the boundary conditions specified according to experimental conditions. The burner-surface separation is 1.06 cm, and the burner and plate temperatures are 423.15 K and 503 K respectively. The exit velocity is 436 cm/s, and species mole fractions of the gas mixture in the nozzle are 3.5% C₂H₄/30% O₂/66.5% Ar (equivalence ratio $\phi = 0.35$) and 580 ppm TTIP, corresponding to a TTIP loading rate of 12 ml/h (this loading rate is used in results hereafter unless otherwise specified). A solution-adapted grid refinement is used in order to achieve convergence with 240–260 grid points. This first step is discussed in detail by Manuputty et al. [18].

In the second step, the resulting gas-phase profile is post-processed with the detailed particle model (Section 3.3.2) to resolve the aggregate particle morphology, solved using a stochastic numerical method. The flame conditions and gas species are supplied as input to the population balance simulation. The simulation requires the computed profiles to be expressed in terms of the residence time of a Lagrangian particle travelling from the burner to the stagnation plate. The combined convective and thermophoretic velocities are used to calculate the particle time history.

The stochastic method employs a direct simulation algorithm (DSA) [24] with a majorant

kernel and fictitious jumps [12, 23] to improve the computational speed of calculating the coagulation rate, and a linear process deferment algorithm [22] to provide an efficient treatment of sintering and condensation. Simulation results in this study are an average of 4 runs with 8192 stochastic particles.

4.2 Particle population governing equations

4.2.1 First simulation

In the first simulation, the particle population balance is coupled to the flow and gas-phase chemistry through the moment transport equations. The transport equation for the r^{th} -moment, M_r , is composed of the moment source, advective, thermophoretic and diffusive transport terms [31]

$$\dot{M}_r - \rho u \frac{d}{dz} \left(\frac{M_r}{\rho} \right) - \frac{d}{dz} (v_T M_r) + \frac{d}{dz} \left(\rho D_{p,1} \frac{d}{dz} \left(\frac{M_{r-2/3}}{\rho} \right) \right) = 0, \quad (1)$$

where ρ is the gas-phase density, v_T is the thermophoretic velocity, and u is the convective velocity. \dot{M}_r is the r^{th} moment source term, z is the spatial displacement along the flame and $D_{p,1}$ is the Brownian diffusion coefficient of a TiO_2 monomer [18].

4.2.2 Second simulation

In the stochastic simulation, the population balance equations are spatially homogeneous. What is simulated is a Lagrangian view of particles in the simulation sample volume travelling with the velocity field. The governing equation for the stochastic population balance is

$$\frac{dn(x)}{dt} = R(x) - \gamma n(x), \quad (2)$$

where $n(x)$ is the number density of particles of type x , and $R(x)$ is their rate of production: a function of the inception, condensation, coagulation and sintering rates. γ is the rate of gas-phase expansion: a function of temperature and the rate of production of gas-phase species.

Expressed in terms of the number density moments of the mass distribution

$$M_r = \sum_{i=1}^{\infty} i^r n_i, \quad (3)$$

the governing equation is

$$\frac{dM_r}{dt} = \dot{M}_r - \gamma M_r, \quad (4)$$

where \dot{M}_r is the moment source term, n_i is the number density of particles of mass $i \cdot m_{\text{TiO}_2}$, with m_{TiO_2} as the mass of a single monomer of TiO_2 .

The stochastic method approximates real particles with a collection of computational particles in a sample volume V_{smp} . The sample volume corresponds to the actual volume

in the real system in which the number of real particles matches the number of computational particles. γ adjusts the sample volume in response to gas-phase expansion and contraction such that

$$\frac{1}{V_{\text{smp1}}} \frac{dV_{\text{smp1}}}{dt} = \gamma. \quad (5)$$

4.2.3 Thermophoretic correction

In order to perform the post-process we need to impose the same conditions on the particle population in the second simulation as modelled in the first. Therefore, the governing equations for both steps of the methodology need to be similar (Eqs. (1) and (4)). The equation for the stochastic simulation (Eq. (4)) does not currently account for thermophoretic and diffusive transport.

If, however, the thermophoretic and diffusive transport effects in the modelled system are small and can be neglected in the post-process it is straightforward to show that the governing equation in second simulation (Eq. (4)) approximates the moment transport equation solved in the first simulation (Eq. (1)). This is the case for premixed laminar flames with no stagnation plate such as those simulated in Refs. [2, 7, 21, 23, 25]. Neglecting the thermophoretic and diffusive transport terms, the moment transport equation (Eq. (1)) becomes

$$\dot{M}_r - \rho u \frac{d}{dz} \left(\frac{M_r}{\rho} \right) = 0. \quad (6)$$

Expressing Eq. (6) in terms of the residence time of a Lagrangian particle by making the coordinate transformation $dz = u dt$ yields the equation for the second simulation (Eq. (4)) with a gas-phase expansion rate

$$\gamma = -\frac{1}{\rho} \frac{d\rho}{dt}. \quad (7)$$

Here, the sample volume adjustment corresponds to the change in gas-phase density i.e. the gas-phase mass contained within the sample volume is conserved (mass transfer to the particle phase is assumed to be negligible).

In the case of a stagnation flame, as modelled in this work, thermophoresis is significant near the cooled stagnation plate due to a steep temperature gradient, so the thermophoretic transport term cannot be neglected. Assuming instead that only the diffusive term is negligible Eq. (1) becomes

$$\dot{M}_r - (u + v_T) \frac{dM_r}{dz} + \left(\frac{u}{\rho} \frac{d\rho}{dz} - \frac{dv_T}{dz} \right) M_r = 0, \quad (8)$$

Using the convective and thermophoretic velocities, we make the coordinate transformation $dz = (u + v_T) dt$ to express Eq. (8) in terms of the residence time of a Lagrangian particle

$$\dot{M}_r - \frac{dM_r}{dt} + \frac{1}{u + v_T} \left(\frac{u}{\rho} \frac{d\rho}{dt} - \frac{dv_T}{dt} \right) M_r = 0, \quad (9)$$

which has the form of the governing equation for the second simulation (Eq. (4)) with

$$\gamma = -\frac{1}{(u + v_T)} \left(\frac{u}{\rho} \frac{d\rho}{dt} - \frac{dv_T}{dt} \right). \quad (10)$$

Thus, the effect of thermophoresis is now accounted for in the volume adjustment term in the stochastic population balance where the convective and thermophoretic velocities, and gas-phase density are supplied as input. Note that setting $v_T = 0$ returns the earlier relation (Eq. (7)).

The diffusive term cannot be dealt with in the same way because it is a second order derivative of the moments and not independent of the PSD. A possible method could be to apply a diffusion correction to the reactor volume for a specific moment order. For example applying the correction for $r = 1$ to ensure the system mass remains in agreement between the two simulations. However, the correction would only be approximate for other moments and is outside the scope of this work.

4.3 Simulated TEM images

The individual primary particle coordinate information tracked in the detailed type-space allows for visualisation of simulated particles. In particular, TEM-style images can be generated by sampling the particle ensemble. Such images can then be compared with experimental TEM micrographs. A TEM-style image is produced using the following algorithm:

1. Uniformly select a particle P_q .
2. Rotate P_q to a random orientation using the method described by Arvo [1].
3. Generate (x, y) coordinates uniformly in the image plane with $-a \leq x \leq a$ and $-b \leq y \leq b$, where a and b define the frame size.
4. Position P_q above the image plane with its centre of mass at (x, y) .
5. Project P_q down onto the image plane.
6. Repeat steps 1–5 for further particles.

5 Results and Discussion

5.1 Transport terms

Figure 5 shows the simulated temperature and velocity profiles obtained from the first step. We observe two regions with significant thermophoresis: at the flame front where the temperature increases steeply; and near the cooled stagnation plate where the temperature rapidly decreases. The region near the stagnation surface is of particular significance

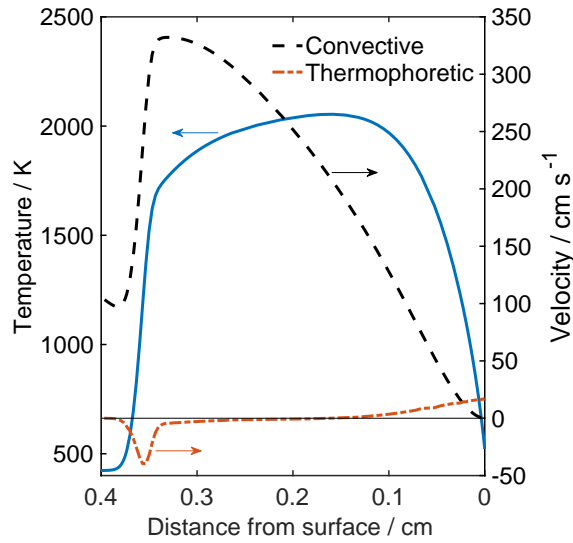


Figure 5: *Temperature and velocity profiles obtained from the first simulation.*

because the convective velocity is low so in the Lagrangian view a particle will spend a large fraction of its residence time here. It is therefore important to correctly account for the effect of transport processes on the particle population dynamics in this region.

In Fig. 6 we compare the relative sizes of the individual terms in moment transport equation (Eq.(1)) solved in the first simulation step. The advection, thermophoresis, diffusion, and moment source terms are shown for the first three moments $r = 0, 1, 2$. The plots show that for a stagnation flame the transport terms are significant and need to be considered in the second step post-process. In particular, the thermophoretic term dominates in the region near the stagnation surface for the higher order moments, and will influence the PSD near the point of experimental measurement.

Diffusion is much less significant at the stagnation surface and can be assumed to be negligible here. However, at the flame front the diffusive term is non-negligible, particularly in the zeroth moment. Here, the convective velocity is very high so in the Lagrangian view diffusive effects will occur over a short period of time early in the evolution of the particle population; thus, the impact of diffusion on the final PSD is likely to be much less significant than thermophoresis.

5.2 Post-processing method evaluation

We can evaluate the effect of applying the thermophoretic correction (Eq. (10)) to the second step simulation by post-processing the flame profile with the spherical particle model and comparing the results of the post-process with the moments calculated in the first simulation. Using the same particle model in both simulation steps eliminates particle model dependent effects on the solutions. For the purpose of comparison, the moments solved by MoMIC in the first simulation are treated as the reference solution because this is the fully coupled simulation solved with transport.

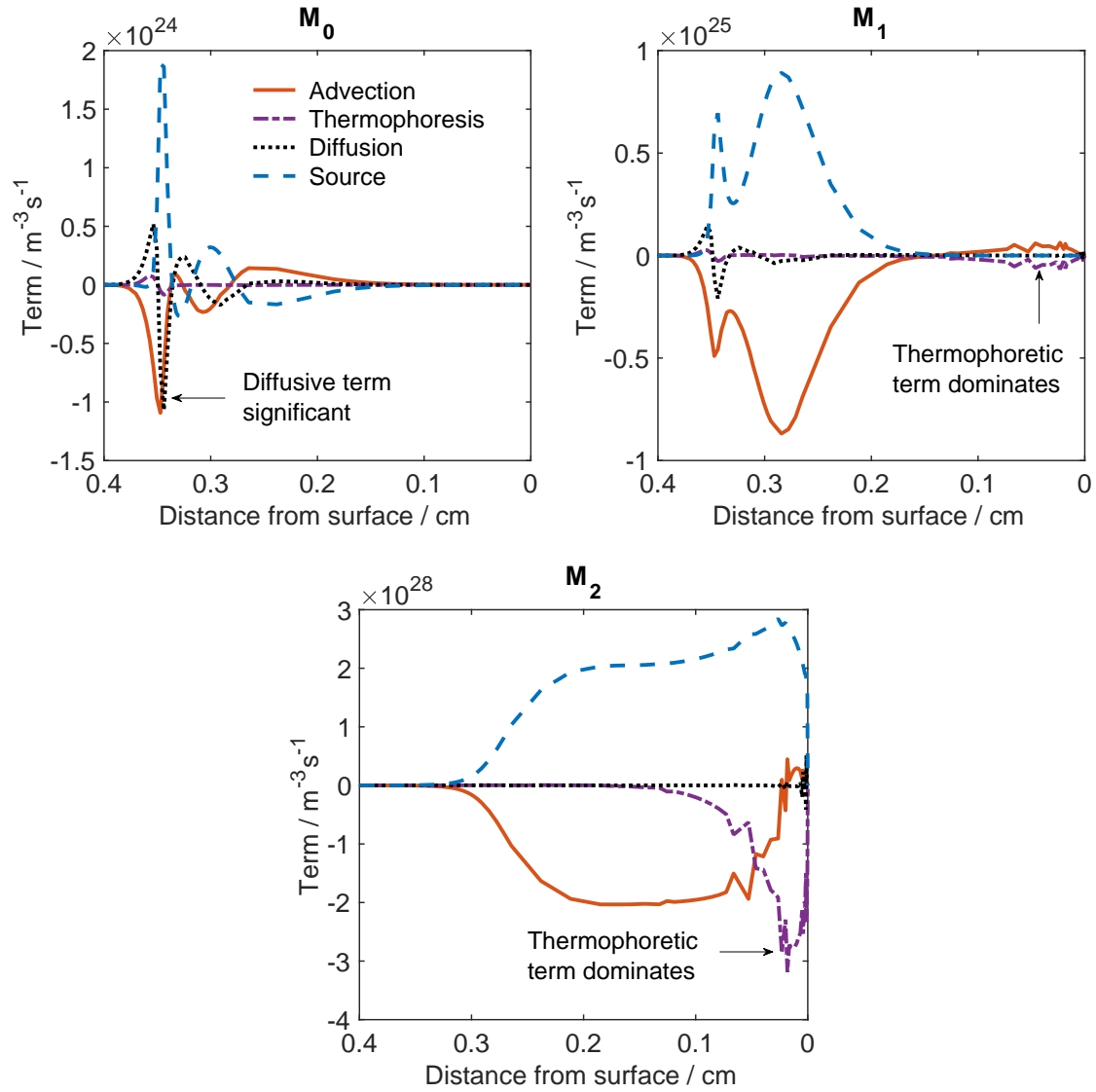


Figure 6: *Moment transport equation terms from the first simulation.*

Figure 7(a) shows the moments obtained by post-processing using the spherical particle model with and without thermophoretic correction, together with the MoMIC reference solution. The Ti(OH)_4 collision species mole fraction is included for reference. The thermophoretic correction was found to significantly improve the agreement between the post-process and the MoMIC reference solution near the stagnation surface (at $z = 0$ cm) where thermophoretic transport effects are most significant.

The large difference in the predicted moments at the flame front is a consequence of the resolution of stochastic method. A statistically significant solution only exists once the concentration of Ti(OH)_4 , the collision species, is high enough and therefore the particle inception rate is large enough for particles to be incepted into the simulation sample volume with reasonable probability.

The relative difference in the moments predicted by the post-process at the stagnation

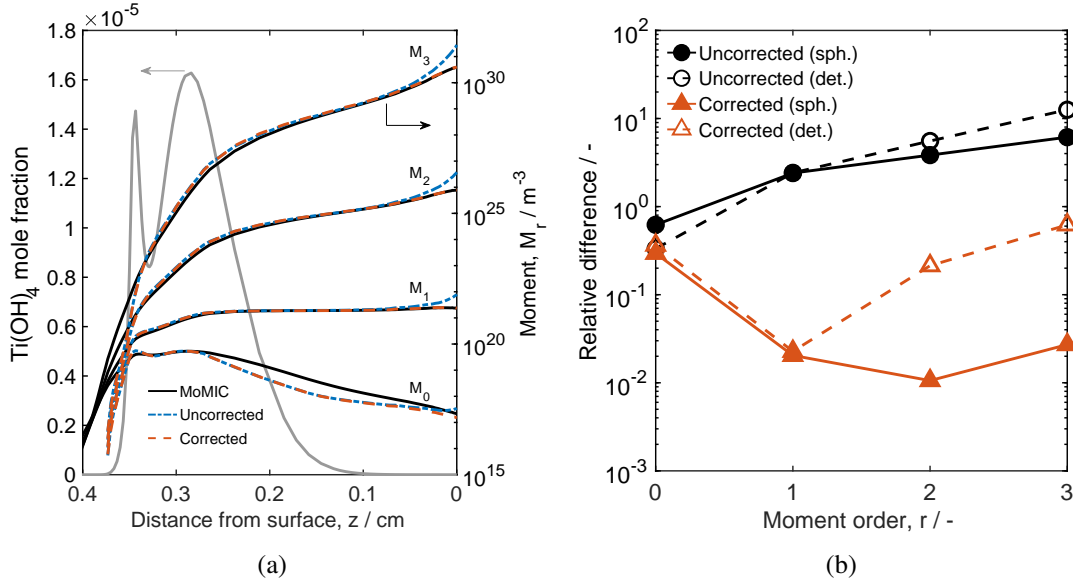


Figure 7: (a) Moments obtained from the first-step MoMIC simulation and from post-processing with a spherical particle model with and without the thermophoretic correction. The $\text{Ti}(\text{OH})_4$ collision species mole fraction is added for reference. (b) The relative difference in the moments at the stagnation surface measured against the MoMIC solution for the spherical (sph.) and detailed (det.) particle models.

surface measured against the MoMIC reference solution is plotted as a function of moment order, r , in Fig. 7(b). Results from post-processing with the spherical and detailed particle model are shown, with and without thermophoretic correction. For $r \geq 1$ a significant reduction in the relative difference is observed with the introduction of the thermophoretic correction for both particle models. Naturally, the spherical particle model shows better agreement (for $r \geq 2$) than the detailed model because a spherical model is also used in the first simulation. The aggregate particle structure described by the detailed model is expected to affect the shape of the predicted PSD, and thus, the higher order moments.

The zeroth moment shows little to no improvement when the thermophoretic correction is introduced. Two possible reasons for this are: the greater relative importance of diffusion on M_0 (Fig. 6); and differences in the numerical methods, especially in the treatment of coagulation. A difference between the two solutions is expected because MoMIC introduces a numerical approximation, while the stochastic method treats coagulation exactly. In particular, the MoMIC calculation of the M_0 source term requires an extrapolated negative order fractional moment [11], which is prone to numerical error. Furthermore, the divergence in M_0 in Fig. 7(a) does not coincide with extrema in the M_0 diffusion term in Fig. 6 suggesting that diffusion is not the cause. At the point of divergence the M_0 diffusion term is negligible. This would suggest that the error arises from differences between the two numerical methods.

Figure 8 shows a comparison of the average particle diameter as a function of TTIP loading for spherical and detailed particle models, with and without the thermophoretic cor-

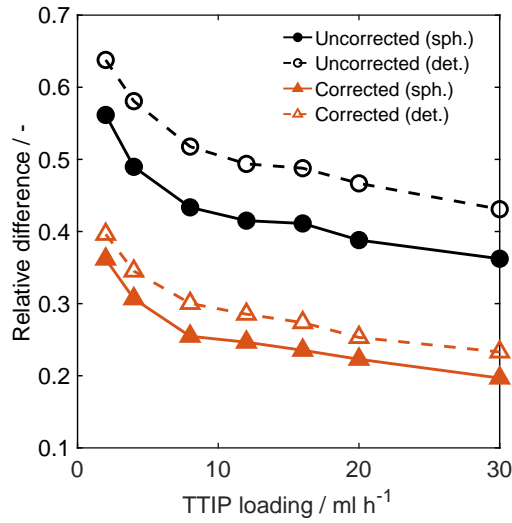


Figure 8: *Relative difference in particle collision diameter measured against the MoMIC reference solution plotted as a function of TTIP loading. Results from post-processing using a spherical particle model (sph.) and detailed particle model (det.) are shown with and without thermophoretic correction.*

rection. For the detailed particle model the collision diameter is calculated as per Lavvas et al. [16]. We see that the thermophoretic correction reduces the error substantially for both spherical and detailed models. However, the difference observed in the zeroth moment in Fig. 7 is carried over into the average particle properties, hence the agreement is not as good as for the individual moments. The plots show a general trend of improving agreement with increased TTIP loading. This is primarily driven by the behaviour of the divergence in M_0 and not an effect of the thermophoretic correction.

5.3 Detailed particle model application

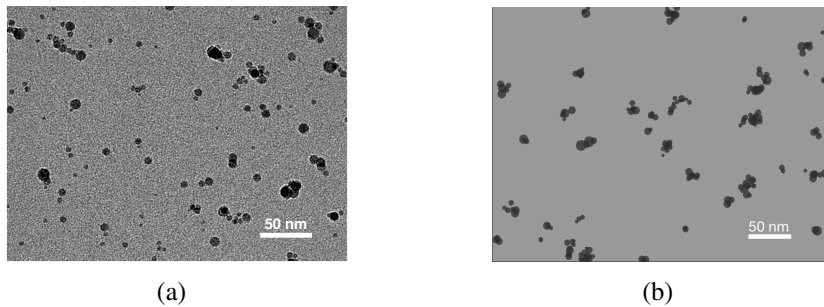


Figure 9: *An experimental TEM image (unpublished data) (a) and a simulated TEM-style image (b).*

Figure 9 shows an experimental TEM image of aggregate TiO_2 particles synthesised in a stagnation flame and a simulated TEM-style image produced under similar modelled con-

ditions. In both images we observe sintered aggregate particles of comparable aggregate and primary size. This illustrates that resolving the aggregate structure and modelling morphology dependent processes such as sintering are important for making proper comparison with experimental results.

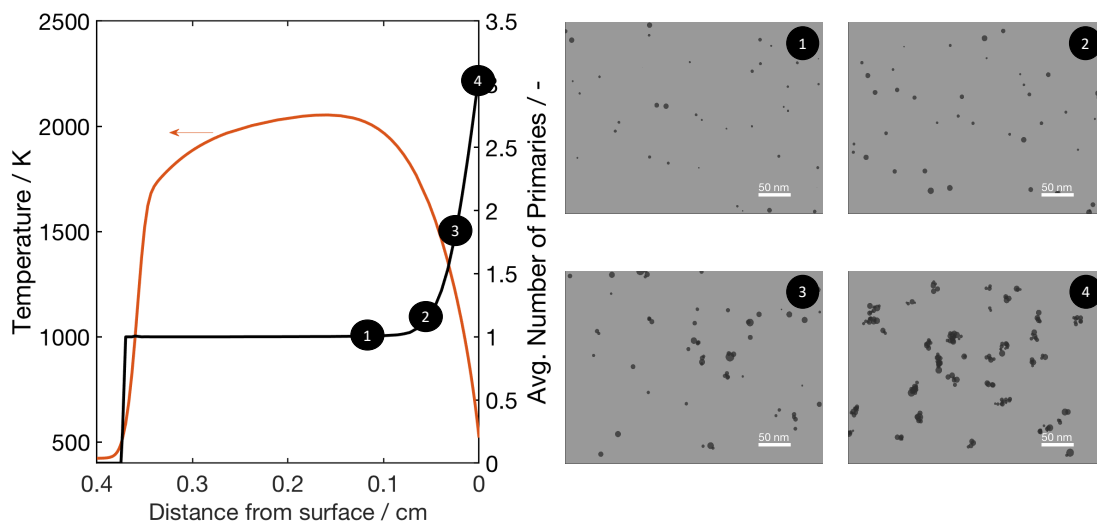


Figure 10: Simulated temperature profile and average number of primaries per aggregate predicted by the post-process. Four simulated TEM-style snapshots are shown at different points along the flame.

In Fig. 10 the average number of primaries per aggregate predicted by the post-process as a function of distance from the stagnation plate is plotted together with the simulated temperature profile. The formation of aggregates is observed as the temperature decreases substantially near the stagnation surface. This is due to the rate of sintering having a stronger temperature dependence than coagulation. The TEM-style snapshots generated at different points along the flame illustrate this change in particle morphology.

6 Conclusions

This paper presented a general two-step modelling methodology able to resolve the complex aggregate morphology of nanoparticles synthesised in a stagnation flame. The methodology was applied to the combustion synthesis of TiO_2 particles from TTIP precursor. A detailed particle model is necessary to simulate the evolution of aggregate particles observed in experiments.

The first step of the two-step methodology couples detailed gas-phase chemistry, a one-dimensional flow model and spherical particle model solved with MoMIC. The resulting flame profile is then post-processed using a detailed particle model capable of tracking individual primary coordinates to resolve the aggregate structure. The method allows for

comparison with experimental observations such as TEM images and enables the study of morphology dependent particle processes.

Examination of the magnitude of the terms in the MoMIC equations showed that thermophoretic transport effects are significant near the stagnation surface and must be accounted for in the second step where the flame profile is post-processed. To do this, a thermophoretic correction to the simulation sample volume was introduced. Comparison of moments predicted by the second-step post-process against the first-step MoMIC solution showed that the thermophoretic correction leads to a significant reduction in the error associated with the post-process. However, a divergence in the zeroth moment was observed, which has an impact on the average particle properties. This is suspected to be caused by differences between the two numerical methods used; in particular, their treatment of coagulation.

7 Acknowledgements

This project is supported by the National Research Foundation (NRF), Prime Minister's Office, Singapore under its Campus for Research Excellence and Technological Enterprise (CREATE) programme. The authors also thank Venator and CMCL Innovations for generous financial support.

References

- [1] J. Arvo. Fast random rotation matrices. In D. Kirk, editor, *Graphics Gems III*, pages 117–120. Academic Press, 1992.
- [2] M. Balthasar and M. Kraft. A stochastic approach to calculate the particle size distribution function of soot particles in laminar premixed flames. *Combust. Flame*, 133:289 – 298, 2003. doi:10.1016/S0010-2180(03)00003-8.
- [3] A. Boje, J. Akroyd, S. Sutcliffe, J. Edwards, and M. Kraft. Detailed population balance modelling of TiO₂ synthesis in an industrial reactor. *Chem. Eng. Sci.*, 164: 219–231, 2017. doi:10.1016/j.ces.2017.02.019.
- [4] P. Buerger, D. Nurkowski, J. Akroyd, S. Mosbach, and M. Kraft. First-principles thermochemistry for the thermal decomposition of titanium tetraisopropoxide. *J. Phys. Chem. A*, 119:8376–8387, 2015. doi:10.1021/acs.jpca.5b01721.
- [5] P. Buerger, D. Nurkowski, J. Akroyd, and M. Kraft. A kinetic mechanism for the thermal decomposition of titanium tetraisopropoxide. *Proc. Combust. Inst.*, 36: 1019–1027, 2017. doi:10.1016/j.proci.2016.08.062.
- [6] J. Camacho, A. V. Singh, W. Wang, R. Shan, E. K. Y. Yapp, D. Chen, M. Kraft, and H. Wang. Soot particle size distributions in premixed stretch-stabilized flat ethylene-oxygen-argon flames. *Proc. Combust. Inst.*, 36:1001–1009, 2017. doi:10.1016/j.proci.2016.06.170.
- [7] D. Chen, Z. Zainuddin, E. Yapp, J. Akroyd, S. Mosbach, and M. Kraft. A fully coupled simulation of pah and soot growth with a population balance model. *Proc. Combust. Inst.*, 34:1827 – 1835, 2013. doi:10.1016/j.proci.2012.06.089.
- [8] CMCL Innovations. kinetics[®], 2016. URL <http://www.cmclinnovations.com/>.
- [9] M. L. Eggersdorfer, D. Kadau, H. J. Herrmann, and S. E. Pratsinis. Multiparticle sintering dynamics: From fractal-like aggregates to compact structures. *Langmuir*, 27:6358–6367, 2011. doi:10.1021/la200546g.
- [10] M. L. Eggersdorfer, D. Kadau, H. J. Herrmann, and S. E. Pratsinis. Aggregate morphology evolution by sintering: Number and diameter of primary particles. *J. Aerosol Sci.*, 46:7–19, 2012. doi:10.1016/j.jaerosci.2011.11.005.
- [11] M. Frenklach. Method of moments with interpolative closure. *Chem. Eng. Sci.*, 57: 2229 – 2239, 2002. doi:10.1016/S0009-2509(02)00113-6.
- [12] M. Goodson and M. Kraft. An efficient stochastic algorithm for simulating nano-particle dynamics. *J. Comput. Phys.*, 183:210–232, 2002. doi:10.1006/jcph.2002.7192.

- [13] J. I. Jeong and M. Choi. A bimodal moment model for the simulation of particle growth. *J. Aerosol Sci.*, 35:1071–1090, 2004. doi:10.1016/j.jaerosci.2004.04.005.
- [14] R. Jullien. Transparency effects in cluster-cluster aggregation with linear trajectories. *J. Phys. A*, 17:L771–L776, 1984. doi:10.1088/0305-4470/17/14/009.
- [15] M. Kraft. Modelling of particulate processes. *KONA Powder Part. J.*, 23:18–35, 2005. doi:10.14356/kona.2005007.
- [16] P. Lavvas, M. Sander, M. Kraft, and H. Imanaka. Surface chemistry and particle shape. Processes for the evolution of aerosols in Titan’s atmosphere. *Astrophys. J.*, 728:80, 2011. doi:10.1088/0004-637X/728/2/80.
- [17] C. Lindberg, J. Akroyd, and M. Kraft. Developing breakage models relating morphological data to the milling behaviour of flame synthesised titania particles. *Chem. Eng. Sci.*, 166:53–65, 2017. doi:10.1016/j.ces.2017.03.016.
- [18] M. Y. Manuputty, J. Akroyd, S. Mosbach, and M. Kraft. Modelling TiO₂ formation in a stagnation flame using method of moments with interpolative closure. *Combust. Flame*, 178:135–147, 2017. doi:10.1016/j.combustflame.2017.01.005.
- [19] S. Memarzadeh, E. D. Tolmachoff, D. J. Phares, and H. Wang. Properties of nanocrystalline TiO₂ synthesized in premixed flames stabilized on a rotating surface. *Proc. Combust. Inst.*, 33:1917–1924, 2011. doi:10.1016/j.proci.2010.05.065.
- [20] W. J. Menz and M. Kraft. A new model for silicon nanoparticle synthesis. *Combust. Flame*, 160:947–958, 2013. doi:10.1016/j.combustflame.2013.01.014.
- [21] N. Morgan, M. Kraft, M. Balthasar, D. Wong, M. Frenklach, and P. Mitchell. Numerical simulations of soot aggregation in premixed laminar flames. *Proc. Combust. Inst.*, 31(1):693 – 700, 2007. doi:10.1016/j.proci.2006.08.021.
- [22] R. I. A. Patterson, J. Singh, M. Balthasar, M. Kraft, and J. R. Norris. The linear process deferment algorithm: A new technique for solving population balance equations. *SIAM J. Sci. Comput.*, 28:303–320, 2006. doi:10.1137/040618953.
- [23] R. I. A. Patterson, J. Singh, M. Balthasar, M. Kraft, and W. Wagner. Extending stochastic soot simulation to higher pressures. *Combust. Flame*, 145:638–642, 2006. doi:10.1016/j.combustflame.2006.02.005.
- [24] S. Shekar, W. J. Menz, A. J. Smith, M. Kraft, and W. Wagner. On a multivariate population balance model to describe the structure and composition of silica nanoparticles. *Comput. Chem. Eng.*, 43:130–147, 2012. doi:10.1016/j.compchemeng.2012.04.010.
- [25] J. Singh, M. Balthasar, M. Kraft, and W. Wagner. Stochastic modeling of soot particle size and age distributions in laminar premixed flames. *Proc. Combust. Inst.*, 30: 1457 – 1465, 2005. doi:10.1016/j.proci.2004.08.120.

- [26] E. D. Tolmachoff, A. D. Abid, D. J. Phares, C. S. Campbell, and H. Wang. Synthesis of nano-phase TiO_2 crystalline films over premixed stagnation flames. *Proc. Combust. Inst.*, 32 II:1839–1845, 2009. doi:10.1016/j.proci.2008.06.052.
- [27] S. Tsantilis and S. E. Pratsinis. Narrowing the size distribution of aerosol-made titania by surface growth and coagulation. *J. Aerosol Sci.*, 35:405–420, 2004. doi:10.1016/j.jaerosci.2003.09.006.
- [28] S. Tsantilis, H. K. Kammler, and S. E. Pratsinis. Population balance modeling of flame synthesis of titania nanoparticles. *Chem. Eng. Sci.*, 57:2139–2156, 2002. doi:10.1016/S0009-2509(02)00107-0.
- [29] H. Wang, X. You, A. V. Joshi, S. G. Davis, A. Laskin, F. Egolfopoulos, and C. K. Law. USC mech version II. High-temperature combustion reaction model of $\text{H}_2/\text{CO}/\text{C}_1\text{-C}_4$ compounds, 2007. URL http://ignis.usc.edu/USC_Mech_II.htm. Accessed on 12 December 2015.
- [30] Z. Xu, H. Zhao, and H. Zhao. CFD-population balance Monte Carlo simulation and numerical optimization for flame synthesis of TiO_2 nanoparticles. *Proc. Combust. Inst.*, 36:1099–1108, 2017. doi:10.1016/j.proci.2016.07.008.
- [31] E. K. Y. Yapp, D. Chen, J. Akroyd, S. Mosbach, M. Kraft, J. Camacho, and H. Wang. Numerical simulation and parametric sensitivity study of particle size distributions in a burner-stabilised stagnation flame. *Combust. Flame*, 162:2569–2581, 2015. doi:10.1016/j.combustflame.2015.03.006.